Numerical investigation of fire in the cavity of naturally ventilated double skin façade with venetian blinds

Youxian Huang[1], Siegfried Yeboah[1,2] (ID) and Jingjing Shao[3] (ID)

Abstract

Double skin façades (DSFs), offer great views, architectural aesthetics, and energy savings. Yet, in a fire event the glass façade breaks leading to risks to human life and firefighting difficulties. Shading devices incorporated to prevent unfavourable heat gains to reduce cooling load though offer energy savings potentially present other challenges in firefighting and occupants' evacuation. In this study, Fire Dynamic Simulator (FDS) was used to numerically investigate the spread of a 5 MW HRR polyurethane GM27 fire in a multi-storey double skin façade building with Venetian blinds placed in its cavity. The blinds were positioned 0.4 m away from the internal glazing, middle of the cavity and 0.4 m away from the external glazing respectively. In each blind position the slat angle was opened at 0°, 45°, 90° and 135° respectively. The results show peak inner glazing surface temperature ranged between 283°C to 840°C depending on the thermocouple position, the Venetian blind position and slat opening angle. Without Venetian blinds, peak inner glazing surface temperatures ranged between 468°C to 614°C. In all cases except when the slat angle was 0° and the blind was positioned closer to the outer glazing, the inner glazing surface temperature from the closest thermocouple (TC 14) above the fire room exceeded 600°C, the glass breakage temperature threshold. Overall, the Venetian blind position and slat opening angle influenced the spread of fire. Venetian blind combustibility and flammability were not considered and therefore recommended for future studies.

Practical Application: Our manuscript helps to develop new thinking on mitigation of fire risks in buildings for architects, engineers and designers when incorporating Venetian blinds in Double Skin Façades (DSFs).

Keywords

Combustion model, double skin façade, fire dynamics simulation, fire safety, venetian blind

Introduction

Background

The façade plays a vital role in buildings, protecting the internal environment and acting as a medium for heat transfer between the indoors and outdoors.[1–3] For conventional buildings, inappropriate materials or techniques chosen for facades can have adverse effects on performance, leading to overheating, poor natural

[1]Department of Architecture and Built Environment, Faculty of Science and Engineering, The University of Nottingham, Ningbo, China
[2]School of the Built Environment and Architecture, London South Bank University, London, UK
[3]Ningbo University of Technology, Ningbo, China

Corresponding author:
Siegfried Yeboah, School of the Built Environment and Architecture, London South Bank University, 103 Borough Road, London SE1 0AA, UK.
Email: yeboahs5@lsbu.ac.uk

ventilation, and excessive energy consumption.[4–7] Double Skin Façades (DSFs) have superseded general glass façades in optimizing building performance while providing great views, better indoor environment, and architectural aesthetics.[8,9] Their double-layer glass allows the reduction of heating and cooling demand while appropriate lighting is permitted indoors to reduce the artificial lighting load.[4,10] For naturally ventilated DSFs, thermal buoyancy, stack effect and wind effect dominate the ventilation process.[11–13]

Influence of venetian blinds on double skin façade performance

To block unfavourable heat gains, DSFs can incorporate shading devices during hot periods to reduce cooling load.[12,14] Typical is the installation of Venetian blinds in its intermediate cavity to influence building performance.[5,15] For instance, Oesterle et al.[16] found that the smaller space created between these shading devices and the glazing heats up, influencing DSF performance. Wang et al.[17] simulated DSFs with the blinds of slat angles 0°, 30°, 60°, and 90° in an air cavity of 0.4 m thick and vent area of 0.3 m^2, and found that Venetian blinds significantly affect the solar radiation transmitted into the indoor environment, impacting the temperature and airflow rate in the cavity. Ji et al.,[18] Jiru et al.[19] and Lee et al.[20] carried out similar simulations and concluded that the cooling energy demand increases with increasing slat angle. Ji et al.[18] found that 80° Venetian blind angle opening performs well and increases natural ventilation by up to 35%. Jiru et al.[19] compared various positions of Venetian blinds in the DSF cavity and found turbulence caused by the blinds intersect with the thermal boundary layer of glazing, leading to enhanced heat transfer when the blinds are close to the glazing. Gratia and De Herde[14] found that cooling consumption in an office building with DSF can be decreased up to 23.2% depending on blind location, blind colour and double skin opening. Iyi et al.[21] also found that the optimum blind position for energy saving is about one-third of the external glazing.

Fire and smoke in the double skin façade system

DSFs although can optimize building energy performance, face challenges complying with fire codes leading to many failing fire safety requirements.[8,22] Shao et al.[23] carried out a Computational fluid dynamic (CFD) analysis on the naturally ventilated DSF at the Center for Sustainable Energy Technologies (CSET) building in Ningbo, China. They found that though it met the national fire safety requirement in China, it still failed to prevent the spread of fire, allowing smoke to occupy the fire exit stairway. According to Abdoh et al.,[6] fire safety in DSFs is crucial due to recent spikes in fires in high rise buildings with DSF systems.

When exposed to fire with a significant heat release rate (HRR), the expansion rate at the centre of the glass in a DSF system becomes more significant than the area protected by the window frame resulting in thermal stress, cracking and subsequent breaking.[24] The smoke entering the cavity between the two panes flows upwards under stack effect, leading to risks to human safety, fast fire spread to upper floors, difficulties for firefighting, and fire debris.[25,26] Ni et al.[25] found that the aluminium frames of windows would deform considerably before the glass broke, resulting in smoke penetrating through the gaps between the pane and frame into the DSF cavity. Their experiment also showed that with 0.7 MW, 1 MW or 2 MW maximum HRRs, a 6-mm-thick, toughened glass glazing would break at glass surface temperatures between 600-800°C.[25] Miao and Chow[27] also found that for a given cavity width, HRR and geometry of window opening are two key factors that influences plume trajectory. Abdoh et al.[6] conducted fire simulation in DSF with the Venetian blinds using smoothed particle method and found that the blind angle could significantly affect fire spread and temperature distribution in the DSF.

Similar to findings by Abdoh et al.,[6] we posit that in addition to blind angle, where Venetian blinds are located in the DSF cavity and their varied combinations with blind angle openings may affect the spread of fire. To this end, we numerically investigated the influence of Venetian blind position and slat opening angle on the spread of fire in the DSF cavity of a multi-storey building using National Institute of Standards and Technology (NIST) Fire Dynamic Simulator (FDS). The purpose is to develop new thinking on mitigation of fire risks in buildings for

architects, engineers and designers when incorporating Venetian blinds in DSFs.

Numerical methodology

Physical and geometrical model

Figure 1(a) and (b) show the physical and geometrical models of the building with multi-storey type DSF spanning 5 floors[28] designed using PyroSim Version 2021.1.0224. The building is 6m deep and 15m high. Each room is 3m high with a 36 m^2 construction area. Windows connecting to the DSF cavity from each room have dimensions of 4×2 m^2. The cavity of the DSF system is 1.2 m deep, with a solar chimney 1m above the building. The widths for Openings 1 and 2 are 1.2 m, respectively. Fresh air enters the naturally ventilated DSF through opening 2 below, and stale air exits via opening 1 above. 200 mm wide Venetian blinds oriented vertically and openable at various slat angles are installed in the DSF cavity. The solar chimney enables a temperature gradient to be established for stack effect. In a fire event, all the openings into the DSF are assumed closed except openings 1 and 2. The fire source, a 1 m^3 burner located at the centre of the room, is on the first floor and 2.5 m away from the DSF inner window. The window in this room is broken to allow hot gas flow into the DSF cavity.

Meshed model

Table 1 shows the mesh data for the simulation. To save computation time, the fire room (MESH01) and the DSF system (MESH02) were meshed separately with different mesh sizes but uniform grid covering all domains relative to the building. The adoption of the uniform grid was aimed at ensuring the stability of the simulation of the fire event.[29] As part of the model validation, mesh sensitivity analysis was carried out similar to work done by Ji et al.[30]

Simulation methodology

The simulation was carried out using Fire Dynamics Simulator (FDS) version 6.7.5. The fuel selected for
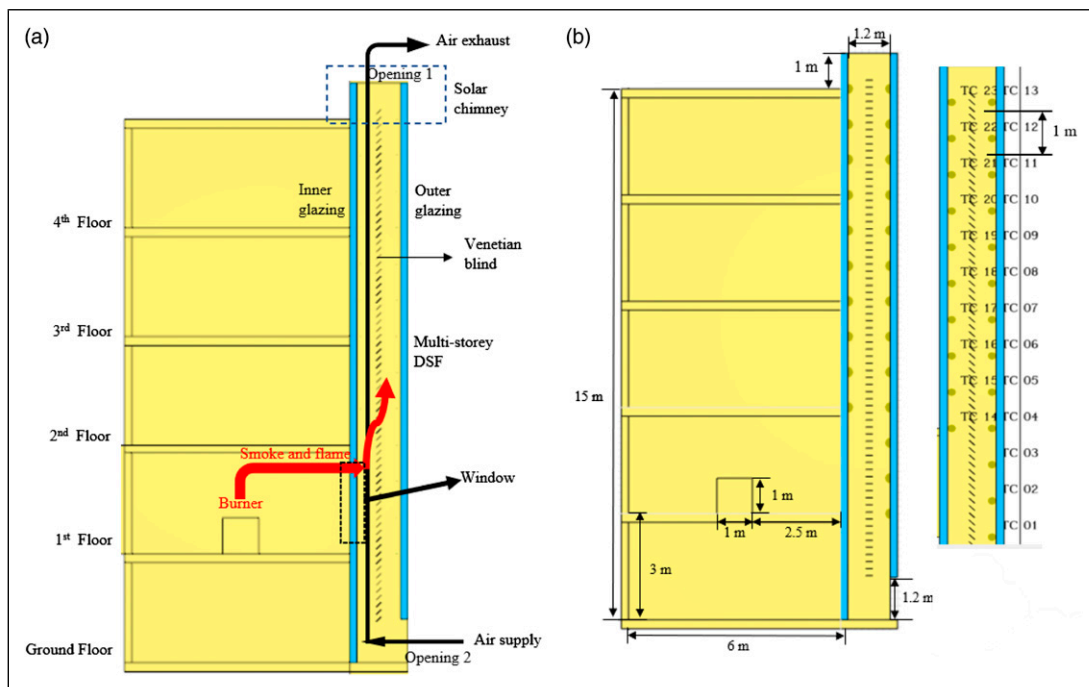
Figure 1. (a) Physical model. (b) Geometrical model showing numbered thermocouple location.

the fire was Polyurethane GM27, consistent with Society of Fire Protection Engineers (SFPE) standards. The burner surface area was 1m2 and to achieve a HRR 5 MW, the heat release rate per area (HRRPUA) for the burner surface was set to 5000 kW/m2. This HRR for the fire scenario is consistent with the fire authorities fire hazard assessment test values[28,31] and it was set to maintain at that HRR value throughout the simulation. The combustion was based on the Mixture Fraction Combustion Model in FDS applicable to the Very Large Eddy Simulation (V-LES) model used for this simulation. V-LES provides a good compromise between efficiency and precision and useful in situations where LES remains computationally expensive under high to very-high Reynolds number flow conditions.[32] For an infinitely fast reaction, FDS sums the lumped species mass production rates and their respective heats of formation to determine the HRR per unit volume as presented in Equation (1).[33]

$$\dot{q}''' = -\sum_a \dot{m}_a''' \Delta h_{f,a} \qquad (1)$$

Thermocouples 0.1 m apart were installed vertically on the inner and outer glazing surfaces corresponding to each floor of the building (See Figure 1(b)). 13 different simulations were carried out for varied Venetian blind positions and slat angle openings, as shown in Table 2. In the DSF cavity, the Venetian blinds were positioned 0.4 m away from the internal glazing, middle of the cavity and 0.4 m away from the external glazing, respectively, for each case investigated. Air leakage, along with the effects of wind and solar radiation, were ignored. A simulation start time of 0.0s and end time of 100s was specified along with a wall update increment of 2 timesteps. The V-LES simulation type was used with a Smagorinsky constant of 0.2 while the Courant–Friedrichs–Lewy (CFL) and Von Neumann Constraints were both respectively maintained at specified minimum of 0.8 and maximum of 1.0.

Table 1. Mesh data.

Zone	Mesh boundary						Grid quality	Grid size (m)
	x_{min} (m)	x_{max} (m)	y_{min} (m)	y_{max} (m)	z_{min} (m)	z_{max} (m)		
Fire room (MESH01)	−0.8	6	−1	7	3	6	34 × 40 × 15	0.2 × 0.2 × 0.2
DSF (MESH02)	6	8	−1	7	−1	17	20 × 80 × 180	0.1 × 0.1 × 0.1

Table 2. Simulated cases.

Case No	Venetian blind angle	Venetian blind position
1	No blinds	No blinds
2	135°	0.4 m away from the internal glazing
3	135°	Middle of the cavity
4	135°	0.4 m away from the external glazing
5	90°	0.4 m away from the internal glazing
6	90°	Middle of the cavity
7	90°	0.4 m away from the external glazing
8	45°	0.4 m away from the internal glazing
9	45°	Middle of the cavity
10	45°	0.4 m away from the external glazing
11	0°	0.4 m away from the internal glazing
12	0°	Middle of the cavity
13	0°	0.4 m away from the external glazing

Results and discussion

Spread of fire in double skin façades without venetian blinds

The investigations begun with the simulation of the 5 MW HRR fire in the DSF without Venetian blind. As shown in Figure 2, the hot gas exited the fire room and attached itself to the interior pane due to high air entrainment from the bottom opening of the DSF. The curvature of the jet increased until the flow attached itself to the inner glazing surface due to Coanda effect.[34] As a result, it was highly likely that interior pane reaching a temperature over 600°C would break allowing flame and smoke to take over immediate upper floors.[6,25]

Hot gas flow in double skin façade with venetian blind

Twelve (12) different cases were simulated respectively to explore the impact of Venetian blinds on the hot gas flow. With the Venetian blinds oriented vertically in the DSF cavity, two zones, Zone 1 and Zone 2 were created. Zone 1 represented the cavity space between the inner glazing and the Venetian blind, and Zone 2 the cavity space between the Venetian blind and the outer glazing of the DSF.

Velocity profile

Slat opening angle = 135°. Figure 3(a)–(c) shows velocity vectors in DSF with Venetian blinds placed 0.4 m away from the inner glazing (Case 2), middle of the DSF cavity (Case 3) and 0.4 m away from the outer glazing (Case 4) respectively. In all three cases, the hot gas flowed through slat opening from Zone 1 into Zone 2. Flow velocities in both Zones increased overtime. Case 2 shows a larger bulk hot gas velocity in Zone 2 reaching a maximum of 7 m/s. Case 3 with the Venetian blind positioned in the middle of the DSF cavity on the other hand shows a larger bulk hot gas velocity in Zone 1 reaching a maximum of 8 m/s. With the Venetian blind closer to the outer glazing (Case 4), a wider Zone 1 was created allowing a larger bulk of hot gas to occupy that zone. For this case, a larger bulk gas velocity reaching a maximum of 9 m/s can be observed in Zone 1. For this slat opening, a larger bulk hot gas velocity is observed in Zone 2 only when the blinds were positioned closer to the inner glazing as in Case 2. Overall, there was unbalanced velocity distribution in the zones with higher air entrainment rate from bottom along the pathway, surging upwards.[28]

Slat Opening Angle = 90°. Figure 4(a)–(c) compares velocity vectors of the hot gas flow through the
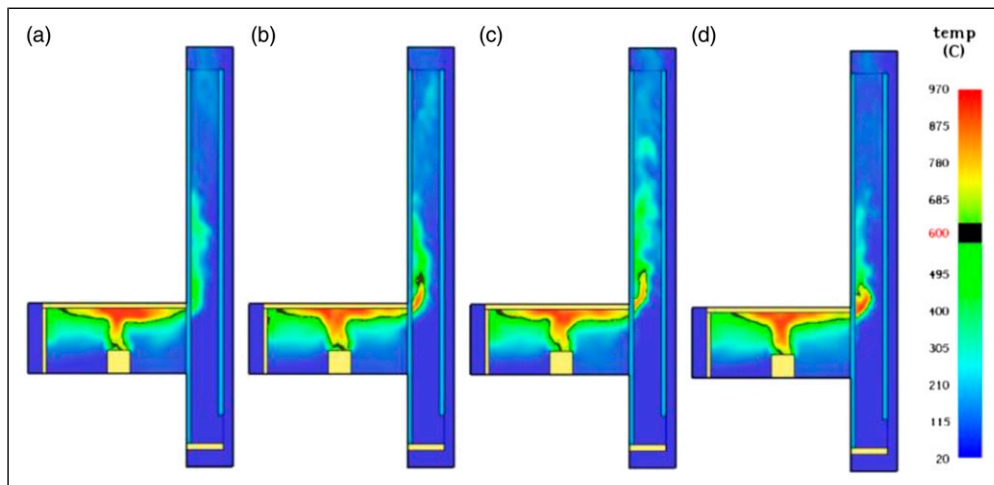
Figure 2. Case 1: Temperature distribution in the DSF system without Venetian blinds (a) at 25s (b) at 50s (c) at 75s (d) at 100s.
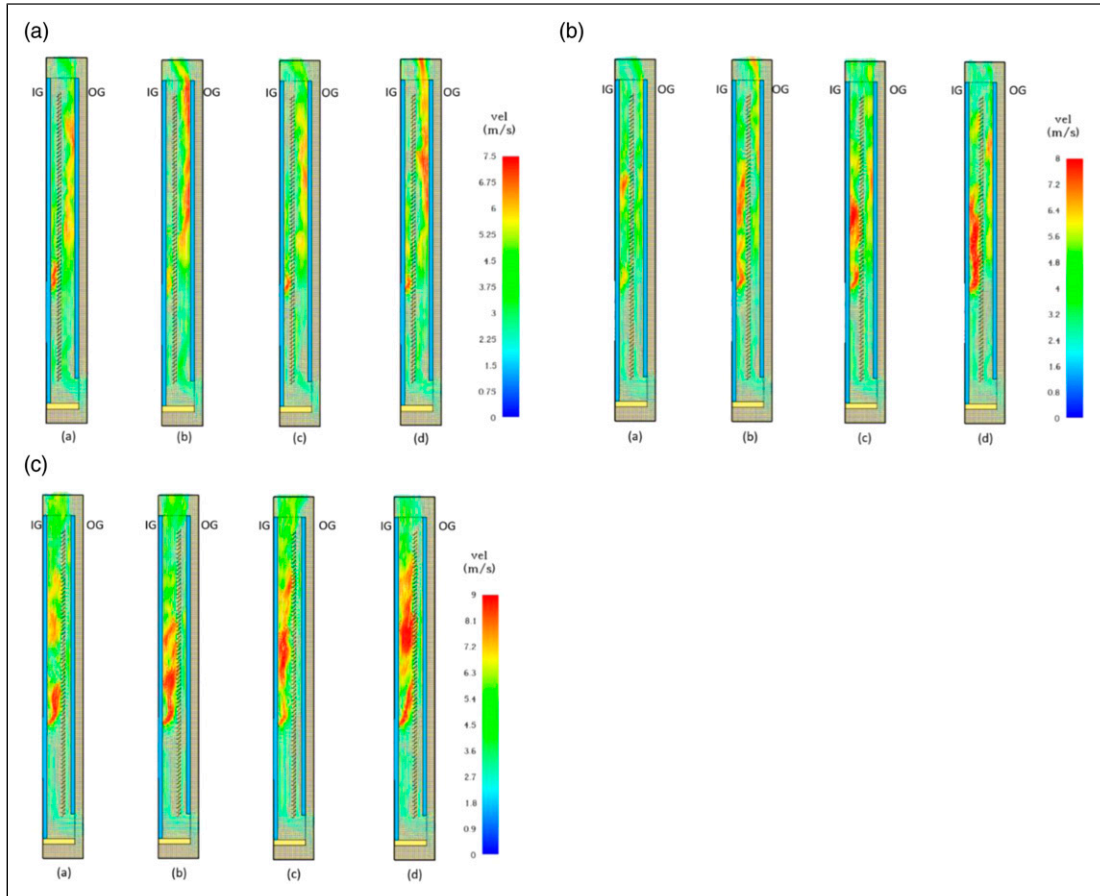
Figure 3. (a) Case 2: Velocity vectors of hot flow in the DSF with Venetian blind opened at 135° - Close to the inner glazing (a) at 25s (b) at 50s (c) at 75s (d) at 100s. (b) Case 3: Velocity vectors of hot flow in the DSF with Venetian blind opened at 135° - In the middle (a) at 25s (b) at 50s (c) 75s (d) at 100s. (c) Case 4: Velocity vectors of hot flow in the DSF with Venetian blind opened at 135° - Close to the outer glazing (a) at 25s (b) at 50s (c) at 75s (d) at 100s.

Venetian blind with slat opened at 90° in the positions represented by Cases 5, 6, and 7 respectively. Like Cases 2–4, as the blind moved closer to outer glazing, flow velocity near the inner glazing increased. In Figure 4(b), unlike Case 3 where the bulk velocity increased in Zone 1, the velocity of the hot flow in both Zones in Case 6 appeared to be balanced. For Cases 5 and 6, maximum hot gas velocity of 8 m/s were observed. In Figure 4(c) the Venetian blind positioned closer to the outer glazing created a larger Zone 1 where the fire plume flowed upward at a comparatively higher velocity. Here, maximum hot gas velocity observed was 9 m/s.

Slat opening angle = 45°. Case 8, Case 9, and Case 10 in Figure 5(a)–(c) shows the velocity profile of DSF with the Venetian blind opened at 45° in the various blind positions. For Case 8, the hot gas flow velocity increased significantly in Zone 2 more than in Zone 1 reaching a maximum of 9 m/s. The increase in the velocity as the hot gas flow exited the Venetian blind opening may be attributable to its acute angle making the opening narrow. The narrow cavity space in Zone 1 appeared to have forced the hot gas to flow through the acute slat opening into Zone 2. Like previous observations in Cases 3 and 6, the bulk velocity of the hot gas in Zone 1 of Figure 5(b) was
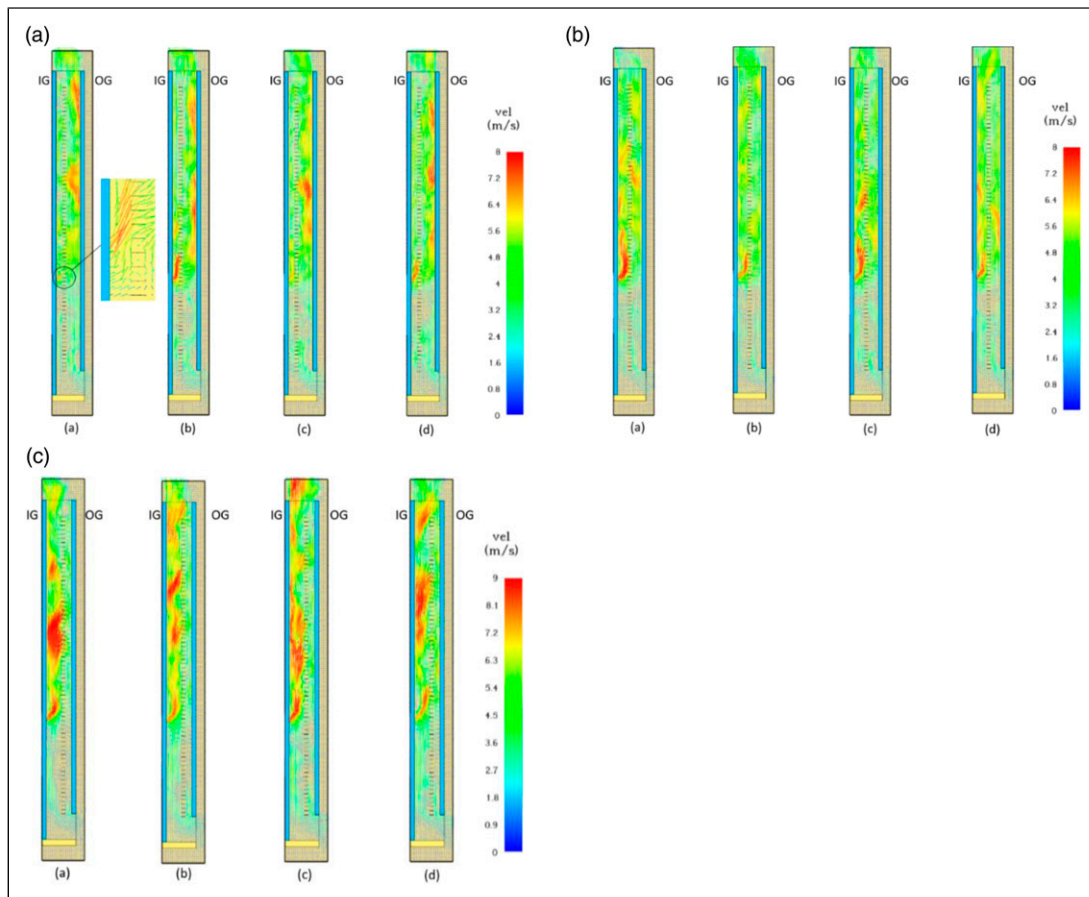
Figure 4. (a) Case 5: Velocity vectors of hot flow in the DSF with Venetian blind opened at 90°- Close to the inner glazing (a) at 25s (b) at 50s (c) at 75s (d) at 100s. (b) Case 6: Velocity vectors of hot flow in the DSF with Venetian blind opened at 90° - in the middle (a) 25s (b) 50s (c) 75s (d) 100s. (c) Case 7: Velocity vectors of hot flow in the DSF with Venetian blind opened at 90° - Close to the outer glazing (a) at 25s (b) at 50s (c) at 75s (d) 100s.

more than that in its Zone 2. It was observed that the acute 45°angle restricted the hot flow moving into Zone 2. Unlike in Case 8 the bulk hot gas flow reaching the maximum velocity of 9 m/s remained largely in Zone 1. In Case 10, the location of the Venetian blind and the acute slat angle allowed a larger buoyant flow in Zone 1 reaching a maximum velocity of 10 m/s.

Overall, most of the hot gases rose with a comparatively low amount going down due to buoyancy indicating that the amount of smoke going to floors lower than the fire location would likely be minimal compared to the amount going to upper floors. Depending on the slat opening angle and the blind position, hot gas

maximum velocities ranged between 7.5 m/s to 10 m/s. In the scenario where the glazing shatters, these maximum hot gas velocities can impact evacuation of occupants leading to firefighting challenges.

Slat Opening Angle = 0°. At 0°slat opening angle, the Venetian blind was fully closed hence acted as a vertical wall dividing the DSF cavity subsequently reducing the cavity space for the hot flow. It is important to note, the Venetian blind was set as incombustible. Overall, the hot flow was observed to mostly move upwards at comparatively higher velocities in Zone 1. For this case, the results show the
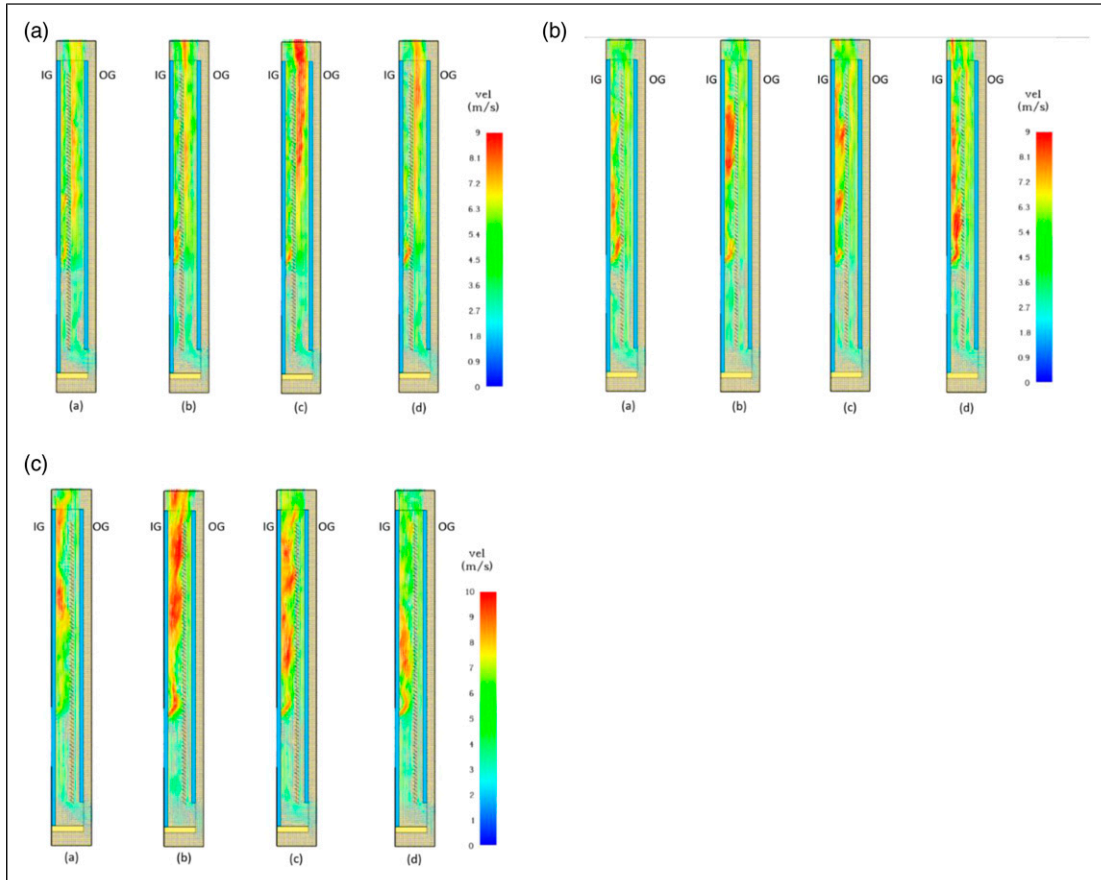
Figure 5. (a) Case 8: Velocity vectors of hot flow in the DSF with Venetian blind opened at 45°- Close to the inner glazing (a) at 25s (b) at 50s (c) at 75s (d) at 100s. (b). Case 9: Velocity vectors of hot flow in the DSF with Venetian blind opened at 45° - In the middle (a) at 25 s (b) at 50 s (c) at 75 s (d) at 100s. (c) Case 10: Velocity vectors of hot flow in the DSF with Venetian blind opened at 45° - Close to the outer glazing (a) at 25 s (b) at 50 s (c) at 75 s (d) at 100s.

influence of the size of the DSF cavity volume on the spread of fire and smoke. Here, irrespective of the size of the cavity dimension created as a result of the blind position, the maximum hot gas velocity reached 10 m/s. This likely will have implications for firefighting and the spread of fire and smoke to immediate upper floors in the event the inner glazing shatters.

Temperature profile

Glazing surface temperatures. Figures 6–9 shows plots for the transient inner and outer glazing surface temperatures for Floor 2 under the simulated scenarios. Floor 2 was chosen as it is immediately above the fire room and significantly impacted due to the pattern of hot gas flow observed in Figure 2. Crucially, the maximum surface temperatures obtained from thermocouples installed on glazing surfaces on Floor 3 and Floor 4 were 471°C and 305°C respectively, both significantly less than the glass breakage threshold temperature of 600°C. On Floor 2 as shown in Figure 1(b), thermocouples TC 04, TC 05, and TC 06 were respectively installed 0.1 m apart on the outer glazing from bottom up. Similarly on the same floor, TC 14, TC 15, and TC 16 were installed 0.1 m apart on the inner glazing.
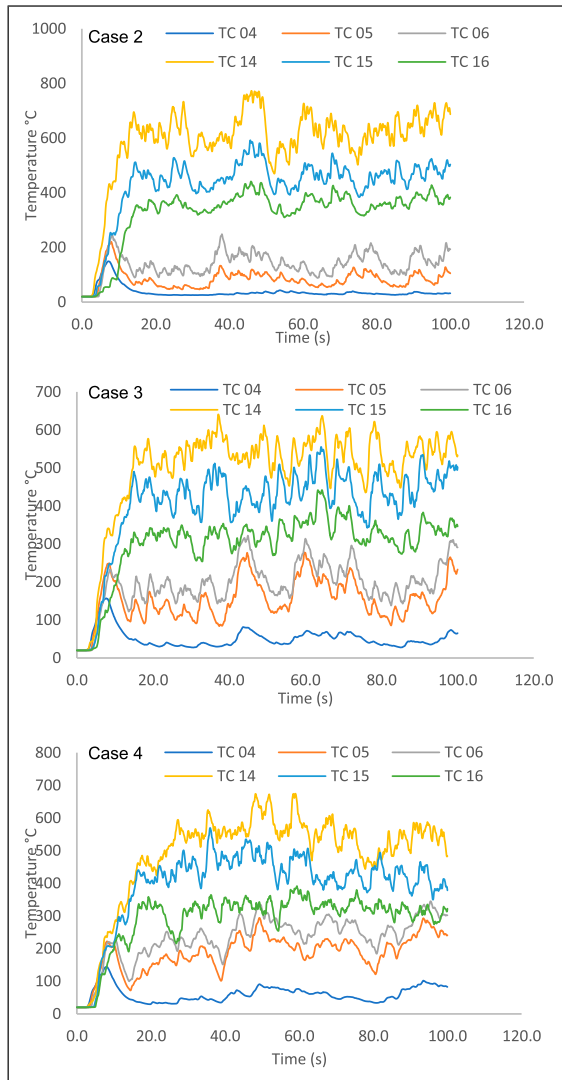
Figure 6. Transient temperature profiles for venetian blind opened at 135°.

In Figure 6, the transient surface temperatures on the Floor 2 glazing with the Venetian blind opened at an angle of 135° is presented. It can be observed that the inner glazing temperature was comparatively higher than the outer glazing temperature for this slat angle opening. In all cases for this slat angle opening, there was a comparatively larger temperature difference between TC 04 and TC 14 the closest thermocouples to the fire room. With TC 14 showing

peak inner glazing surface temperatures above 600°C, it is safe to assume that under this scenario, the inner glazing will shatter allowing smoke and fire to spread to the second floor. For Cases 2, 3 and 4, the peak temperatures obtained for TC 14 were 773°C, 641°C and 675°C respectively. With the time taken for the threshold to be reached, it is also safe to say this could lead to evacuation challenges as hot gases can impact occupants safe exit of the floor. Thermocouple temperatures recorded for TC 15 and TC 16, 0.1 m apart, both above TC 14 shows peak temperatures below the glass breakage threshold. For Case 2 the peak temperatures for TC 15 and TC 16 were 592°C and 442°C respectively. For Case 3 they were 555°C and 442°C respectively while for Case 4 they were 569°C and 391°C respectively. It was also observed that the Venetian blind position at this slat angle opening influenced the amount of the hot gases that occupied Zone 2 to increase the outer glazing surface temperature.

Figure 7 shows Cases 5, 6 and 7 with the Venetian blind angle opened at 90°. Here too, TC 14 over time exceeds the glass breakage threshold. For Case 5, a significant temperature difference between TC 04 and TC 14 was observed throughout the simulation. The difference between the peak surface temperatures for TC 04 (189°C) and TC 14 (700°C) was determined to be 511°C. For TC 05 and TC 15, the temperature difference is comparatively smaller with a peak temperature difference of 71°C. However, the results for TC 06 and TC 16 shows that the outer glazing surface temperature supersedes the inner glazing surface temperature. Here, peak surface temperatures obtained were 348°C and 283°C respectively for TC 06 and TC 16. This shows that more hot gases impinged on the outer glazing surface at that thermocouple level as the hot gases rushed through the 90° slat opening angle. For Case 6, a comparatively larger temperature difference between the peaks of TC 05 (345°C) and TC15 (601°C) was observed. For TC 06 and TC 16, the temperature appears to be similar with only a slight difference between them. Here, peak temperatures for TC 06 and TC 16 were respectively 357°C and 434°C resulting in a peak temperature difference of 77°C. Case 7 on the other hand shows clear temperature differences between the inner glazing surfaces and
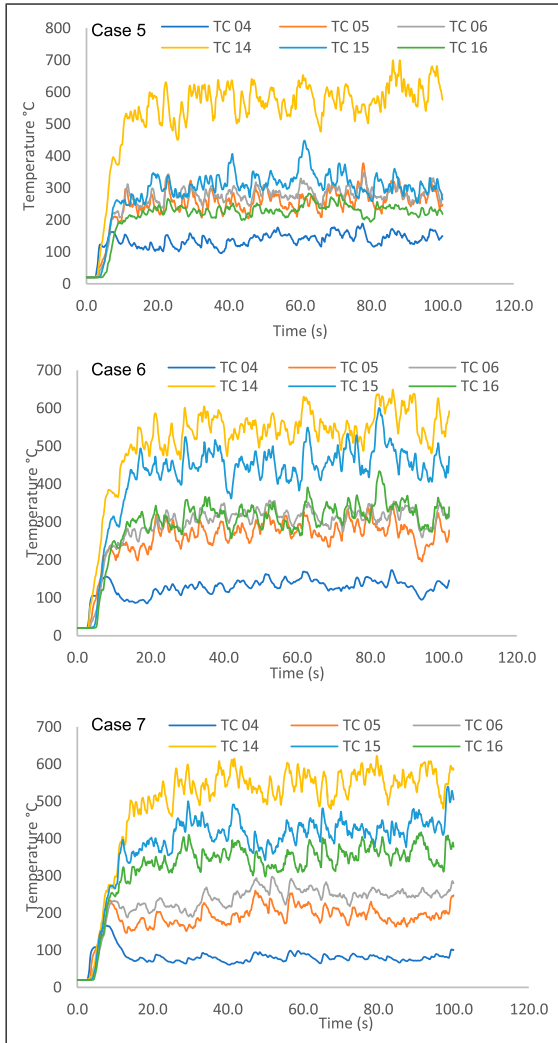
Figure 7. Transient temperature profiles for venetian blind opened at 90°.

outer glazing surfaces. The peak temperatures for TC 04 and TC 14 were 166°C and 622°C respectively. For TC 05 and TC 15, the peak temperatures were 260°C and 539°C respectively. While for TC 06 and TC 16 they were 298°C and 417°C respectively. Here, the recorded temperatures for the inner glazing surfaces overall were comparatively higher than those for the outer glazing surfaces.

Figure 8 shows the transient temperature profiles for Cases 8, 9 and 10 when the Venetian

blind angle was opened at 45°. The results show significantly lower temperatures record on the outer glazing surfaces compared to the cases in Figures 6 and 7. This appears to indicate that at this blind angle opening, the hot gas path to Zone 2 was impeded hence the significant temperature differences between the inner and outer glazing surfaces. For all three cases, peak temperatures for TC 14 and TC 15 were observed to exceed the glass breaking temperature threshold of 600°C. For Cases 8, 9 and 10, TC 14 attained peak temperatures of 840°C, 689°C and 681°C respectively, while TC 15 attained corresponding peak temperatures of 667°C, 677°C and 607°C. For TC 16, the peak temperatures under the three cases were 535°C, 554°C and 517°C respectively, all below the glass breakage temperature threshold. The outer glazing in all three cases achieved peak temperatures comparatively lower and ranging between 59°C and 166°C. With most of the peak temperatures for the inner glazing exceeding the glass breakage threshold, there is the likelihood of the inner glazing shattering. This coupled with a comparatively lower outer glazing temperature can create challenges for firefighting from the outside and occupants' safe evacuation due to the spread of hot gases when the inner glazing shatters.

Figure 9 shows the transient glazing surface temperatures when the Venetian blind was assumed closed. Here, it is important to note that the Venetian blind was specified to be incombustible hence acted as a fire barrier when the slat angle was 0°. For Cases 11 and 12, the peak surface temperatures for TC 14 were 780°C, and 652°C respectively, exceeding the glass breakage temperature threshold. For Case 13, the peak inner glazing surface temperature was below the glass breakage threshold temperature. Here, TC 14, TC 15, and TC 16 registered peak surface temperatures of 598°C, 546°C and 471°C respectively. Since the hot gases did not penetrate the Venetian blind, the outer glazing temperature maintained the initial room temperature set value of 20°C. Overall, the results indicate that the inner glazing surface temperature increased with a decrease in the cavity volume of the zone. This implies that the DSF cavity dimension influences the glazing
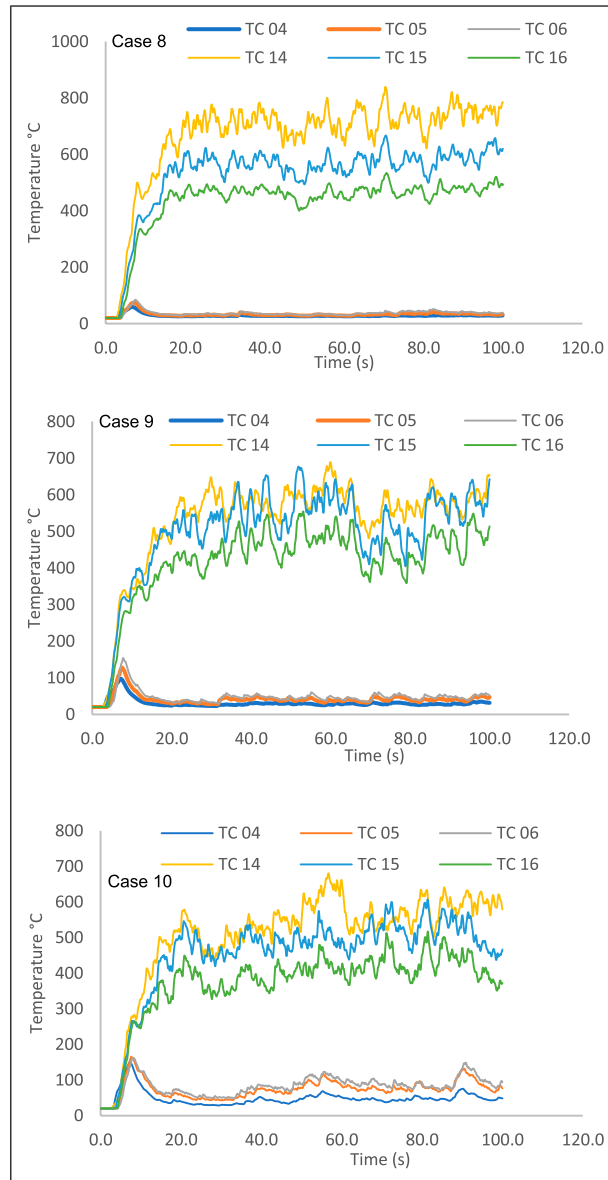
Figure 8. Transient temperature profiles for venetian blind opened at 45°.

surface temperature in a fire event and in this context, it was the inner surface glazing temperature.

Model validation and sensitivity analysis

Validation of model. Since we investigated a fire event invariably of high consequence and uncertainty, we acknowledge that there may be large uncertainties tied to our simulation inputs that may be far from an actual future scenario[35]. The challenges associated with validation of fire models is well recognized due to the high cost and other difficulties of conducting large-scale fire tests[36]. According to Chow et al.[36], most field models are validated by experiments not
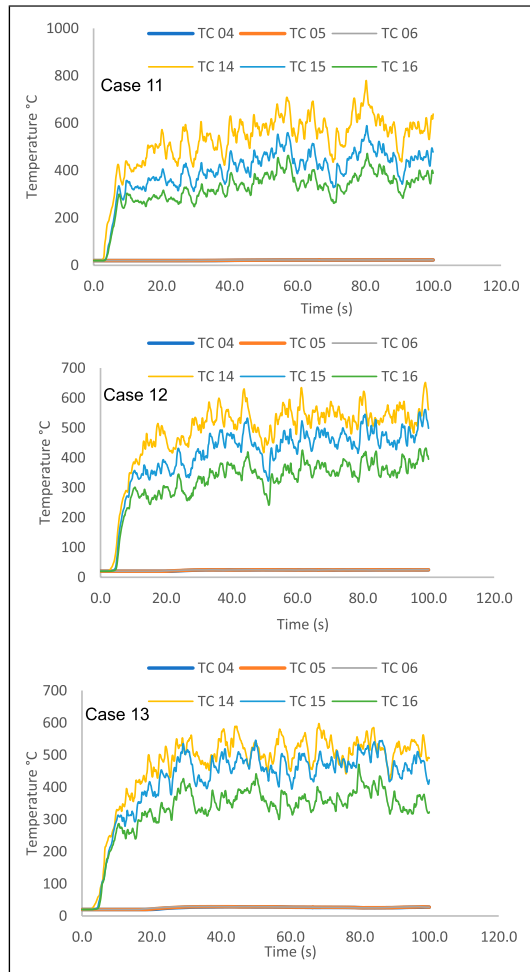
Figure 9. Transient temperature profiles for venetian blind opened at 0°.

specially designed for such purpose with very few studies comparing models with field measurements in actual sites. To this end, we discuss the validation of our model in terms of a historical statement of the model's capability, due to the challenges in replicating the actual fire scenarios in an actual site.[35] As outlined in Pretrel et al.[37] and Merci et al.,[38] challenges in validating numerical fire models makes it necessary for modifications to be made to be able to validate against historical experimental data. Since in this present study there was no actual experimental set up for the validation, we validated our model's

capability by using it input parameters and approach to simulate Peng et al.[39]'s model as a basis of comparison to demonstrate reliability of our results. Peng et al.[39] carried out experimental and numerical studies of fire and smoke movement in the cavity of a double-skin glass façade similar to this present study. They used an FDS model to simulate one of the experimental tests to investigate the effect of fire sources and cavity depths and found good agreement between their experimental and numerical results.

Here, we used our key parameters and approach to model the building in Peng et al.,[39] which is a 2-storey DSF building of dimensions $4 \times 9 \times 3.3$ m high with a DSF cavity depth of 860 mm. The 2-storey building was meshed similarly as our present study, with the fire room meshed with grid size of $0.2 \times 0.2 \times 0.2$ m (MESH 01) and the cavity meshed with grid size of $0.1 \times 0.1 \times 0.1$ m (MESH 02) both with respective grid quality as shown in Table 1. Since Peng et al.[39] did not consider Venetian blind in the cavity of the DSF, we also omitted the Venetian blind in this validation process to enable a reasonable comparison to be made. The Heat Release Rate (HRR) was set as 2 MW, and the simulation was run for 1000s similar to one of the experimental fire scenarios in Peng et al.[39] The HRR was set to develop a fast t^2 growth rate to reach and maintain 2 MW HRR similar to the numerical simulation in Peng et al.[39] The internal facade of the fire room was assumed to be broken. Temperature sensors were placed 0.1 m apart on the inner façade from a height of 1.6 m from ground.

In Figure 10(a) and (b), three plots namely Experimental Results,[39] FDS Model Results,[39] and *FDS Validation Study* are represented on each chart. In our *FDS Validation Study*, we find that simulating Peng et al.[39]'s model with our parameters yielded results that follows closely the experimental results obtained by Peng and co-workers. Although in some situations our *FDS Validation Study* model over-predicted the experimental results obtained by Peng et al.,[39] we still draw confidence in our model's capability to reasonably predict the potential trend under experimental conditions albeit with some level of uncertainty.

As shown in Table 3, the Peak temperatures, and the corresponding times between our *FDS Validation*
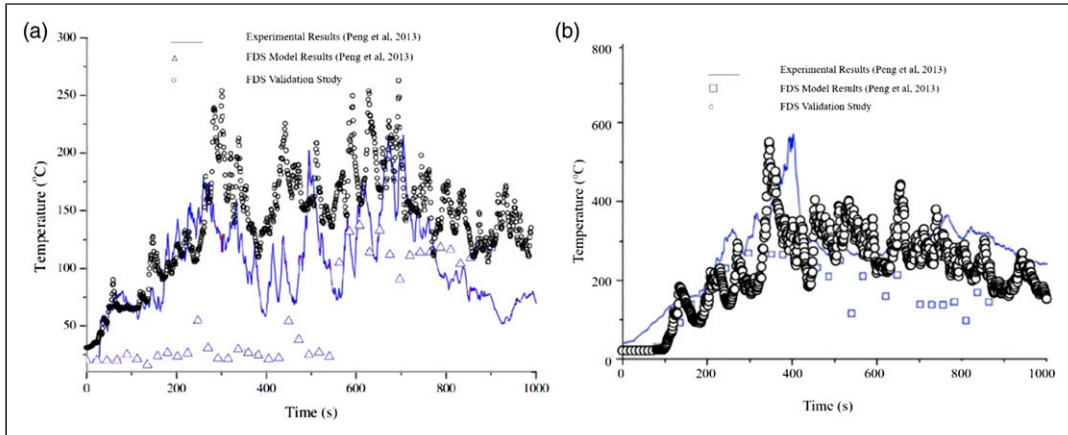
Figure 10. (a) Measured temperature - upper floor. (b) Measured temperature - lower floor.

Table 3. Model validation - results comparison.

Study	Peak temperature (lower floor/upper floor)	Peak temperature time (lower floor/upper floor)
Experimental results [39]	600°C/215°C	400s/700s
FDS model results [39]	230°C/148°C	300s/600s
FDS Validation Study	536°C/263°C	363s/694s

Study and the results from Peng et al.[39] were reasonably close further demonstrating our model's capability to replicate the experimental scenario.

Sensitivity analysis. The mesh statistics for the three different grid sizes used are presented in Table 4. Figure 11 shows mesh sensitivity plots for the temperature profile of TC 14 under the 5 MW HRR fire. B1 is a coarser mesh while B2 and B3 are refined finer mesh sizes. B1 being a coarser mesh, used less computing time; however, the finer meshes, B2 and B3 resulted in significant computation time for the simulation. Results of B2 and B3 were comparatively close with inconsequential differences. For this reason, B2 was chosen for the simulation due to its comparatively less expensive computation time and similarity in the results. It is also obvious from Figure 11 that using Mesh B2 slightly underpredicts the temperature following the same physics. With meshes B2 and B3, relative stability was obtained, and both converged by the

end of the simulation process at 100s as can be seen in Figure 11.

Limitations of study

There were several limitations in this investigation alongside the main limitation of having no real-life experimental model for validation. The first key limitation was to do with PyroSim and FDS using only a rectilinear grid type. This created some challenges as the Venetian blinds with slat angle opening of 45° and 135° could not be meshed directly. This is because the grid did not match the edge, hence, saw tooth domains had to be created as a workaround which influenced the results obtained for those slat angle openings. The other limitation was that although bulk velocity distribution was considered in the simulation as an important fluid flow variable, the pressure distribution in the DSF cavity was not considered. This is because, in the present study, the emphasis was largely on investigating the façade peak temperatures reaching the glass breakage threshold and

Table 4. Statistics for mesh sensitivity analysis.

Case no.		Grid quality	Grid size (m)	Total running time (h: min: s)
MESH02	B1	10 × 40 × 90	0.2 × 0.2 × 0.2	4:26:34
	B2	20 × 80 × 180	0.1 × 0.1 × 0.1	16:31:57
	B3	40 × 160 × 360	0.05 × 0.05 × 0.05	170:07:52
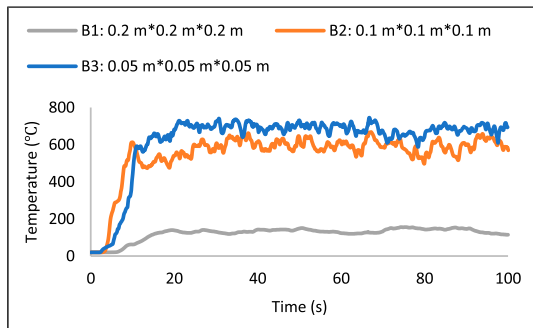
Figure 11. Mesh sensitivity analysis - thermocouple (TC 14) temperature.

related implications. Future studies therefore can consider pressure distribution of the hot gases and its impacts on evacuation in the scenarios investigated. Also, influences from external environmental factors such as wind and solar radiation on the DSF system were ignored although in real life those are factors that cannot be ignored.[5] There were several other assumptions made that potentially influenced the results as well. For instance, air leakage from rooms and DSF system were not taken into consideration. The building was also assumed empty with no mechanical systems.

Conclusion

A numerical investigation of fire in the cavity of a multi-storey naturally ventilated DSF with Venetian blinds was carried out using Fire Dynamic Simulator (FDS). The results show that:

- The bulk hot gas velocities in the DSF cavity zones were influenced by the slat angle opening and blind position. For the scenarios investigated, the maximum bulk hot gas velocities ranged between 7.5 m/s and 10 m/s. The maximum velocity of 10 m/s was observed when the slat angle was 45°and the blind position was 0.4 m away from the outer glazing. While the lowest maximum of 7.5 m/s in the range occurred when the slat angle was 135° and the blind was positioned closer to the inner glazing.
- In the DSF without Venetian blinds, the fire was found to attach itself to the inner glazing due to Coanda effect with a significantly larger air entrainment gap at the bottom. The peak inner glazing surface temperatures obtained ranged between 468°C to 614°C.
- Peak temperatures on the inner glazing surface, ranged between 283°C to 840°C, varying with the position of the thermocouple, the Venetian blind position and slat angle opening. Peak temperatures for TC 14, the closest thermocouple on the floor above the fire room, exceeded the glass breakage temperature of 600°C for all cases except when the Venetian blind was completely closed and placed 0.4 m away from the external glazing, indicating the fire risk levels of the immediate floor above the fire room for a fire of 5 MW HRR.
- At a slat angle of 45°, the Venetian blind acted as a partial fire barrier allowing a small quantity of hot gases to move towards the outer glazing. At 0° slat angle, the Venetian blind completely blocked off the fire preventing it from influencing the surface temperature of the outer glazing on the assumption that the blind material was incombustible. In both cases there were significant surface temperature differences between the inner and outer glazing with the outer glazing surface remaining at significantly lower temperatures.

Overall, the simulation shows that the room immediately above the fire room is exposed to significant fire hazards in the event of a fire as the trajectory

of the fire goes up due to the stack effect. For the same HRR, the Venetian blind position was found to influence the level of temperature increase within the cavity and on the surface of the inner glazing. While the slat angle opening influenced the path of the hot gas flow from Zone 1 to Zone 2 influencing the bulk hot gas velocity distribution in the DSF cavity.

In this, study the combustibility and flammability of various Venetian blind materials were not considered. It would be interesting to know how much influence the rate of combustibility and flammability of such materials will have on the spread of fire and smoke in the DSF; hence we recommend for future studies along with supporting experimental study.

Declaration of conflicting interests

The author(s) declared no potential conflicts of interest with respect to the research, authorship, and/or publication of this article.

Funding

Credit author statement

Huang Youxian: Investigation, Methodology, Writing-Original Draft, Validation. Yeboah, Siegfried: Conceptualization, Supervision, Visualization, Writing - Original Draft, Writing- Reviewing and Editing. Shao, Jingjing: Conceptualization, Writing- Reviewing and Editing, Validation, Funding acquisition.

ORCID iDs

Siegfried Yeboah ⓘD https://orcid.org/0000-0003-4308-9829
Shao Jingjing ⓘD https://orcid.org/0000-0003-3497-7330

References

1. Pérez G., Coma J., Sol S., et al. Green facade for energy savings in buildings: The influence of leaf area index and facade orientation on the shadow effect. *Appl Energy* 2017; 187: 424–437. DOI: 10.1016/j.apenergy.2016.11.055

2. Ghaffarianhoseini A., Ghaffarianhoseini A., Berardi U., et al. Exploring the advantages and challenges of double-skin façades (DSFs). *Renew Sustainable Energy Rev* 2016; 60: 1052–1065. DOI: 10.1016/j.rser.2016.01.130

3. Tovarović J.Č., Ivanović-Šekularac J. and Šekularac N. Renovation of existing glass facade in order to implement energy efficiency and media facade. *Energy Build* 2017; 152: 653–666. DOI: 10.1016/j.enbuild.2017.07.049

4. Li J., Xing X., Hu C., et al. Numerical studies on effects of cavity width on smoke spread in double-skin facade. *Proced Eng* 2012; 45: 695–699. DOI: 10.1016/j.proeng.2012.08.225

5. Shameri M.A., Alghoul M.A., Sopian K., et al. Perspectives of double skin façade systems in buildings and energy saving. *Renew Sustainable Energy Rev* 2011; 15: 1468–1475. DOI: 10.1016/j.rser.2010.10.016

6. Abdoh D.A., Kodur V.K.R. and Liew K.M. Smoothed particle hydrodynamics modeling of the thermal behavior of double skin facades in fires considering the effects of venetian blinds. *Appl Math Model* 2020; 84: 357–376. DOI: 10.1016/j.apm.2020.02.033

7. Saroglou T., Theodosiou T., Givoni B., et al. A study of different envelope scenarios towards low carbon high-rise buildings in the Mediterranean climate - can DSF be part of the solution? *Renew Sustainable Energy Rev* 2019; 113: 109237. DOI: 10.1016/j.rser.2019.06.044

8. Chow W.K. and Hung W.Y. Effect of cavity depth on smoke spreading of double-skin façade. *Building Environ* 2006; 41: 970–979. DOI: 10.1016/j.buildenv.2005.04.009

9. Ding W., Hasemi Y. and Yamada T. Natural ventilation performance of a double-skin façade with a solar chimney. *Energy and Buildings* 2005; 37: 411–418. DOI: 10.1016/j.enbuild.2004.08.002

10. Chow W.K., Hung W.Y., Zuo G., Dong H., Gao Y. et al. Preliminary experimental study of double-skinned façade. *International Journal on Engineering Performance-Based Fire Codes*, 2004; 6(3): 155–167.

11. Wang R.Q., He S.J. and Yue H.R. Numerical study of smoke spread upon shaft-box type double skin facades, *Proced Eng*. 2018. 211: 755–761. DOI: 10.1016/j.proeng.2017.12.072

12. Poirazis H. (2004). Double Skin Façades for Office Buildings-Literature Review. Lund, Sweden. ISBN 91-85147-02-8. https://www.ebd.lth.se/fileadmin/energi_byggnadsdesign/images/Publikationer/Bok-EBD-R3-G5_alt_2_Harris.pdf

13. Loncour X., Deneyer A., Blasco M., Flamant G., Wouters P. and Agent O. (2005). Ventilated Double Skin Façades Classification & illustration of façades concepts Air Infiltration and Ventilation Centre Ventilated Double Skin Façades Classification & illustration of façade concepts. AIVC Contributed Report 3, 2005, 49 pp. Brussels, Belgium. Available at: http://www.bbri.be

14. Gratia E. and De Herde A. The most efficient position of shading devices in a double-skin facade. *Energy and Buildings* 2007; 39: 364–373. DOI: 10.1016/j.enbuild.2006.09.001

15. Zeng Z., Li X., Li C., et al. Modeling ventilation in naturally ventilated double-skin façade with a venetian blind. *Building Environ* 2012; 57: 1–6. DOI: 10.1016/j.buildenv.2012.04.007

16. Oesterle E., Lieb R.-D., Martin L. and Heusler W. 2001. Double-skin façades: integrated planning. Prestel. 1st edition., München, Germany: Prestel. ISBN 10: 3791325043.

17. Wang Y., Chen Y. and Li C. Airflow modeling based on zonal method for natural ventilated double skin façade with Venetian blinds. *Energy and Buildings* 2019; 191: 211–223. DOI: 10.1016/j.enbuild.2019.03.025

18. Ji Y., Cook M.J., Hanby V., et al. CFD modelling of naturally ventilated double-skin facades with Venetian blinds. *J Building Perform Simulation* 2008; 1: 185–196. DOI: 10.1080/19401490802478303

19. Jiru T.E., Tao Y.-X. and Haghighat F. Airflow and heat transfer in double skin facades. *Energy and Buildings* 2011; 43: 2760–2766. DOI: 10.1016/j.enbuild.2011.06.038

20. Lee K.H., Kim T., Lee G., et al. Cooling load reduction effect and its mechanism in between-glass cavity and venetian blind operation during the summer season. *Building Simulation* 2013; 6: 351–364. DOI: 10.1007/s12273-013-0124-9

21. Iyi D., Hasan R., Penlington R., et al. Double skin façade: Modelling technique and influence of venetian blinds on the airflow and heat transfer. *Appl Therm Eng* 2014; 71: 219–229. DOI: 10.1016/j.applthermaleng.2014.06.024

22. Chow W.K., Hung W.Y., Gao Y., et al. Experimental study on smoke movement leading to glass damages in double-skinned façade. *Construction Building Mater* 2007; 21: 556–566. DOI: 10.1016/j.conbuildmat.2005.09.005

23. Shao J., Yeboah S.K., Zhu T., et al. Simulation study on the spreading of fire-induced smoke in natural-ventilated double-skin facade buildings. *Environ Sci Eng* 2020: 1011–1018. DOI: 10.1007/978-981-13-9528-4_102

24. Shields J., Silcock G.W.H. and Flood F. Behaviour of double glazing in corner fires. *Fire Technology* 2005; 41: 37–65. DOI: 10.1007/s10694-005-4629-3

25. Ni Z., Lu S. and Peng L. Experimental study on fire performance of double-skin glass facades. *J Fire Sci* 2012; 30: 457–472. DOI: 10.1177/0734904112447179

26. Chow C.L. Full-scale burning tests on double-skin façade fires. *Fire Mater* 2013; 37: 17–34. DOI: 10.1002/fam.1127

27. Miao L. and Chow C.L. A study on window plume from a room fire to the cavity of a double-skin façade. *Appl Therm Eng* 2018; 129: 230–241. DOI: 10.1016/j.applthermaleng.2017.09.125

28. Chow C.L. Numerical Studies on Smoke Spread in the Cavity of a Double-skin Façade/Skaitinis Dūmų Sklidimo Dvigubo Fasado Ertmėje Tyrimas. *J Civil Eng Management* 2011; 17: 371–392. DOI: 10.3846/13923730.2011.595075

29. Shen T.-S., Huang Y.-H. and Chien S.-W. Using fire dynamic simulation (FDS) to reconstruct an arson fire scene. *Building Environ* 2008; 43: 1036–1045. DOI: 10.1016/j.buildenv.2006.11.001

30. Ji J., Li Y.F., Shi W.X., et al. Numerical studies on smoke spread in the cavity of a double-skin façade. *J Civil Eng Management* 2015; 22: 470–479. DOI: 10.3846/13923730.2014.897992

31. Chow C.L. and Chow W.K. Fire safety aspects of refuge floors in supertall buildings with computational fluid dynamics. *J Civil Eng Management* 2009; 15: 225–236. DOI: 10.3846/1392-3730.2009.15.225-236

32. Labois M. and Lakehal D. Very-Large Eddy Simulation (V-LES) of the flow across a tube bundle. *Nucl Eng Des* 2011; 241: 2075–2085. DOI: 10.1016/j.nucengdes.2011.02.009

33. McGrattan K., Hostikka S., Floyd J., McDermott R. and Vanella M. (2020). Fire dynamics simulator technical reference guide 1; Gaithersburg, MD, 2020. https://doi.org/10.6028/NIST.SP.1018e6.

34. Zhivov A., Skistad H., Mundt E., Posokhin V., Ratcliff M., Shilkrot E., Strongin A., Li X., Zhang T., Zhao F., Shao X. and Yang Y. (2020). Principles of air

and contaminant movement inside and around buildings. In Industrial Ventilation Design Guidebook (pp. 245–370). Elsevier. https://doi.org/10.1016/B978-0-12-816780-9.00007-1

35. Borg A., Paulsen Husted B. and Njå O. The concept of validation of numerical models for consequence analysis. *Reliability Eng Syst Saf* 2014; 125: 36–45. DOI: 10.1016/j.ress.2013.09.009

36. Chow W.K., Li S.S., Gao Y., et al. Numerical studies on atrium smoke movement and control with validation by field tests. *Building Environ* 2009; 44: 1150–1155. DOI: 10.1016/j.buildenv.2008.08.008

37. Pretrel H., Le Saux W. and Audouin L. Determination of the heat release rate of large scale hydrocarbon pool fires in ventilated compartments. *Fire Saf J* 2013; 62: 192–205. DOI: 10.1016/j.firesaf.2013.01.014

38. Merci B., Li J. and Maragkos G. On the importance of the heat release rate in numerical simulations of fires in mechanically ventilated air-tight enclosures. *Proc Combust Inst* 2022. DOI: 10.1016/j.proci.2022.06.011

39. Peng L., Ni Z. and Huang X. Experimental and numerical study of fire spread upon double-skin glass facades. *MATEC Web of Conferences* 2013; 9: 03009. DOI: 10.1051/matecconf/20130903009

Appendix

Notation

f	Body force, N
$h_{f,a}$	Specific enthalpy, kJ/kg
$\dot{m}_a'''$	Lumped species mass production rates, kg/s
$\dot{q}'''$	Heat release per unit volume, kW/m^3
T_i	Average temperature of inner glazing, °C
T_o	Average temperature of outer glazing, °C
ΔT	Temperature difference between the inner glazing temperature and outer glazing temperature, °C

Abbreviations

HHR	heat release rate
HRRPUA	heat release rate per area
FDS	fire dynamic simulator
DFS	double skin facade
CFD	computational fluid dynamics
LES	large Eddy simulation
DNS	direct numerical simulation
IG	inner glazing
OG	outer glazing